

1
2
3
4
5
6
7
8
9
10
11
12
13
14
15
16
17
18
19
20
21
22
23
24
25
26
27
28
29
30
31
32
33
34
35
36
37
38
39
40
41
42
43
44
45
46
47
48
49
50
51
52
53
54
55
56
57
58
59
60
61
62
63
64
65

Theoretical study on naphthobischalcogenadiazole conjugated polymer systems and C61 derivative as organic photovoltaic semiconductors

Takehiro Fujita^a, Toru Matsui^{a,*}, Masato Sumita^{a,b}, Yutaka Imamura^c, and Kenji Morihashi^a

^aDepartment of Chemistry, Graduate School of Pure and Applied Sciences, University of Tsukuba, 1-1-1, Tennodai, Tsukuba, Ibaraki 305-8571, Japan. ^bCenter for Advanced Intelligence Project, RIKEN Nihonbashi 1-chome Mitsui Building, 15th floor, 1-4-1 Nihonbashi, Chuo-ku, Tokyo, 103-0027, Japan. ^cDepartment of Chemistry, Graduate School of Science and Engineering, Tokyo Metropolitan University, 1-1 Minami-osawa, Hachioji, Tokyo 192-0397, Japan.

*Corresponding author, E-mail address: matsui@chem.tsukuba.ac.jp

1
2
3 **Abstract**
4
5

6 We investigated the charge-transfer reactions of solar cells including a quaterthiophene
7 copolymer with naphtho-bis-thiadiazole (PNTz4T) and naphtho-bis-oxadiazole
8 (PNOz4T) using constrained density functional theory (CDFT). According to our
9 calculations, the high electron-transfer rate results in a highly efficient solar cell, and the
10 stable charge-transfer state results in low energy loss. Our computations imply that the
11 following three factors are crucial to improve the performance of semiconducting
12 polymers: (i) large structural changes following charge-transfer, (ii) narrow band gap, and
13 (iii) spatially delocalized lowest unoccupied molecular orbital (LUMO) of the ground
14 state.
15
16
17
18
19
20
21
22
23
24
25
26
27
28
29
30
31
32
33
34
35
36
37
38

39 **Keywords**
40

41 density functional theory; semiconducting polymers; charge transfer; solar cells
42
43
44
45
46
47
48
49
50
51
52
53
54
55
56
57
58
59
60
61
62
63
64
65

1
2
3 **1. Introduction**
4
5

6 Polymer-based bulk-heterojunction solar cells (PSCs) [1] are a type of organic
7 photovoltaic cells (OPVs). Although dye-sensitized solar cells [2] suffer from sealing
8 defects because they utilize liquid electrolytes, PSCs are expected to function effectively
9 as durable solid photoelectric conversion devices. The implementation of polymer films
10 in PSCs as the charge transport material makes them superior to inorganic solar cells in
11 terms of weight and cost. However, two key issues must be addressed before PSCs can be
12 used in practice. The first is their low power conversion efficiency (PCE) relative to
13 inorganic solar cells, and the second is their large energy loss (E_{loss}) [3] (0.7–0.8 eV) as
14 solar energy is converted into electric power.
15
16
17
18
19
20
21
22
23
24
25
26
27
28
29
30
31
32
33
34

35 Although PSCs have several problems generating free electron–hole pairs from sunlight,
36 one method to improve their low PCE and large E_{loss} is to effectively combine their
37 constituent materials. PSCs consist of two types of organic semiconductors with many π
38 electrons; that is, hole transport and electron transport materials with electron-donating
39 and electron-accepting properties, respectively. Current PSCs are composed of
40 polycyclic aromatic hydrocarbons or π -electron conjugated (semiconducting) polymers
41 as the hole transport materials and fullerene derivatives as the electron transport materials.
42
43
44
45
46
47
48
49
50
51
52
53
54
55
56
57
58 Charge recombination [4], which negatively affects charge-transfer, is assumed to be the
59
60
61
62
63
64
65

1
2
3 main cause for the low PCE of PSCs. For materials with low bulk electrical conductivity,
4
5
6 charge recombination is attributed to unstable electron–hole pairs. Therefore, it is helpful
7
8
9 to analyse several combinations of hole transport and electron transport materials to
10
11
12 better understand their electronic structure.
13
14
15

16 To increase the PCE of PSCs, semiconducting polymers [5-7] have been developed in
17
18 the framework of two essential aspects; one is to control the thin film structure, such as its
19
20 crystallinity and orientation, so as to enhance the efficiency of charge transport, whereas
21
22 the other aspect is to control the polymers' electronic structure, such as the absorption
23
24 wavelength and the energy levels of the frontier orbitals, which are important for exciton
25
26 formation. Regarding the electronic structure, a semiconducting polymer with a narrow
27
28 band gap and deep highest occupied molecular orbital (HOMO) level is preferable to
29
30 widen the absorption region and increase the open circuit voltage. Osaka *et al.* reported an
31
32 effective copolymer based on quaterthiophene and naphtho-bis-thiadiazole (PNTz4T) [8],
33
34 with the PCE of PNTz4T with [6,6]-phenyl-C61-butyric acid methyl ester (PCBM)
35
36 (PNTz4T/PCBM) reaching more than 10%. In addition, they also reported a
37
38 quaterthiophene and naphtho-bis-oxadiazole copolymer (PNOz4T) [9]. Both PNTz4T
39
40 and PNOz4T have a high crystallinity, narrow band gap, and deep HOMO level.
41
42 Although the PCE of the PSC with PNOz4T was relatively low (9%), PNOz4T has
43
44
45
46
47
48
49
50
51
52
53
54
55
56
57
58
59
60
61
62
63
64
65

1
2
3 received considerable attention, particularly because of its small E_{loss} (0.53–0.55 eV).
4
5

6 Although clarifying the difference between PNTz4T/ and PNOz4T/PCBM will be helpful
7
8
9 to develop more efficient materials, experiments are often not suitable to observe details
10
11
12 of the charge-transfer process.
13
14
15

16 To this end, quantum chemical analyses are a powerful tool to obtain detailed
17
18
19 understanding of charge-transfer processes. However, conventional density functional
20
21
22 theory (DFT) struggles to describe the charge-transfer states where positive and negative
23
24
25 charges are localized in the hole transporting and electron transporting materials. This
26
27
28 shortcoming of several exchange–correlation DFT functionals results from
29
30
31 self-interaction error (SIE) [10], which includes unphysical electron interactions in the
32
33
34 energy evaluation.
35
36
37

38 Constrained density functional theory (CDFT) of Deberich *et al.* [11,12] is an effective
39
40
41 tool for solving charge-localized systems. CDFT can minimize the energy of the system
42
43
44 under the constraint that the charges and spins remain localized in particular regions of
45
46
47 the system by adding a Lagrange multiplier to the conventional Kohn-Sham DFT
48
49
50 equations. Wu *et al.* developed CDFT further by reporting a way to efficiently explore the
51
52
53 diabatic potential energy curves in Marcus' electron-transfer theory [13], as well as a way
54
55
56 to accurately predict the driving force and reorganization energy [14]. Indeed, using Wu's
57
58
59
60

1
2
3 approach, a lot of electron-transfer reactions were explained [15-17] by computing the
4
5
6 electron-transfer rate constant within the Condon approximation [18]. Because of this
7
8
9 success, we adopted CDFT to estimate the charge-transfer reactions in PSCs.
10

11
12 This study aims to understand the qualitative differences between PNTz4T and PNOz4T
13
14 by comparing the electron-transfer rates (k_{ET}) and the stability of the charge-transfer state
15
16 between PNTz4T/PCBM and PNOz4T/PCBM. Moreover, we also investigated the
17
18
19 conformational dependence of these molecular species on k_{ET} .
20
21
22
23
24
25
26
27

28 29 **2. Method**

30 31 **2.1. Modelling**

32
33
34
35 In this study, we used a donor/acceptor complex extracted from the interface between
36
37 bulk PCBM and PNTz4T/PNOz4T. PNTz4T or PNOz4T was adopted as the electron
38
39 donor, and PCBM [19] was chosen as the electron acceptor, as in the experiments of
40
41
42 Osaka *et al.* [9]. The PCBM model systems with PNTz4T or PNOz4T were prepared as
43
44
45
46
47
48 follows. First, PNTz4T and PNOz4T were orientated face-on to PCBM at the interfaces,
49
50
51 and the polar substituents of PCBM were directed toward the bulk region due to
52
53
54 electrostatic repulsion. Hence, we created the donor–accepter complex models as shown
55
56
57
58 in Figure 1a. The initial structures were prepared to ensure that the nearest distance
59
60
61
62
63
64
65

1
2
3 between the donor and acceptor atoms was approximately 4.0 Å. (see the SI for the
4
5
6 detailed initial structures.) For computational convenience, PNTz4T and PNOz4T were
7
8
9 modelled as monomers by replacing the alkyl chains with methyl groups, which are
10
11
12 hereafter termed NTz4T and NOz4T, respectively. We found that these small model
13
14
15 systems are sufficiently representative of the actual systems to reproduce the three
16
17
18 relevant electronic states of the system (i.e. before light irradiation, after exciton
19
20
21 formation, and after charge-transfer).
22
23
24

25
26 Additionally, we prepared six models for each NTz4T/PCBM and NOz4T/PCBM
27
28 complex (Figure 2) by rotation around the C₂ axis (Figure 1b) to examine their
29
30
31 conformational dependence on k_{ET} . These models are hereafter referred to as **s1-s6**. As
32
33
34 shown in Figure 1b, PCBM was placed above the thiophene rings or the carbon-carbon
35
36
37 bonds of NTz4T or NOz4T.
38
39
40
41
42
43
44
45
46
47
48
49
50
51
52
53
54
55
56
57
58
59
60
61
62
63
64
65

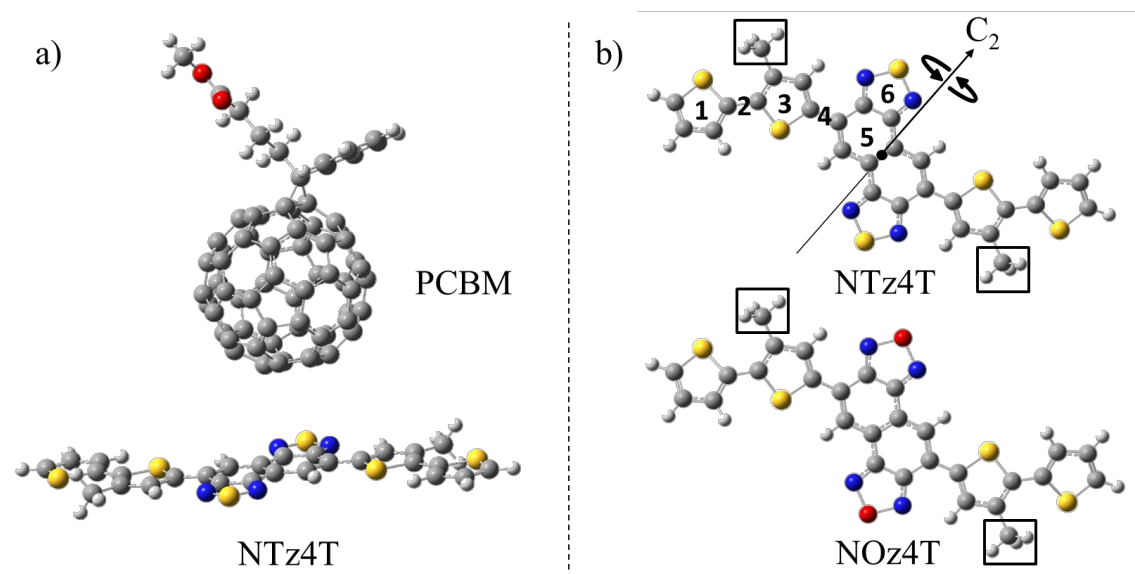


Figure 1. (a) Model of the NTz4T complex with PCBM (NTz4T/PCBM). Blue, red, yellow, white, and grey spheres indicate nitrogen, oxygen, sulfur, hydrogen, and carbon atoms, respectively. (b) Structures of NTz4T and NOz4T. PCBM is placed above the NTz4T or NOz4T moieties and labelled from **1** to **6**, as depicted as **s1-s6** in Figure 2. Face-on conformations were ensured by enforcing C_{2h} symmetry of NTz4T/NOz4T.

2.2. Geometry Optimization and Single-Point Energy Calculations

All calculations in this study were performed using the B3LYP [20] hybrid density functional and the 6-31G(d) basis set. The total energy of these models was determined through the following three steps: (i) all-atom geometry optimization of the ground state, (ii) geometry optimization of each molecule, and (iii) single-point energy calculations.

All models were optimized using GAUSSIAN 09 [21]. Only the donor was extracted from

1
2
3 the optimized structures of **s1-s6**, and geometry optimizations of the singlet ground and
4
5
6 excited states and the radical cation state were performed. Time-dependent DFT
7
8
9 (TD-DFT) [22] as implemented in GAUSSIAN 09 was used to calculate the singlet excited
10
11
12 state. For PCBM, geometry optimizations of the singlet ground and radical anion states
13
14
15 were also performed. These optimized molecules were then combined while maintaining
16
17
18 their ground-state interatomic distances. Finally, single point-energy calculations were
19
20
21 performed using our own CDFT program [15-17]. After the charge-transfer was
22
23
24 calculated for each system, the constraint was set to ensure charges of +1 and -1 for the
25
26
27 donor and acceptor, respectively.
28
29
30
31
32
33
34

35 **2.3. Electron Transfer Rate and Stabilization Energy**

36
37
38 The electron-transfer rate constants, k_{ET} , were calculated using Equation (1) [23]:
39
40
41
42
43

$$44 \quad k_{\text{ET}} = \frac{4\pi^2}{h} \frac{|H_{\text{ab}}|^2}{\sqrt{4\pi\lambda k_{\text{B}}T}} \exp\left(-\frac{(\Delta G^0 + \lambda)^2}{4\lambda k_{\text{B}}T}\right) \quad (1)$$

45
46
47
48
49
50

51 where h , k_{B} , and T are Planck's constant, Boltzmann's constant, and absolute temperature,
52
53
54 respectively. The driving force (ΔG^0), reorganization energy (λ), and electron coupling
55
56
57 constant (H_{ab}) were calculated from the energy and orbitals obtained by single-point
58
59
60

1
2
3 energy calculations at the CDFT level of theory. k_{ET} was determined with $T = 300$ K and
4
5
6 H_{ab} was calculated based on the theory proposed by Wu *et al.* [18]. Because CDFT
7
8
9 struggles to describe singlet excited states, H_{ab} was approximated by assuming that the
10
11
12 triplet excited state is equal to the singlet excited state.
13
14
15

16 Hereafter, we use the standard notation $E(a|b)$ to represent the energy in the “ a ” state
17
18 with the equilibrium structure in the “ b ” state. For example, each energy of the system
19
20 before light irradiation, after exciton formation, and after charge-transfer is expressed as
21
22 $E(\text{DA}|\text{DA})$, $E(\text{D}^*\text{A}|\text{D}^*\text{A})$, and $E(\text{D}^{+\bullet}\text{A}^{-\bullet}|\text{D}^{+\bullet}\text{A}^{-\bullet})$, respectively. Here, D and A indicate the
23
24 donor and acceptor, respectively. ΔG^0 was obtained approximately from the difference
25
26 between the internal energies of the systems as follows:
27
28
29
30
31
32
33
34
35
36
37

$$\Delta G^0 \cong E(\text{D}^{+\bullet}\text{A}^{-\bullet}|\text{D}^{+\bullet}\text{A}^{-\bullet}) - E(\text{D}^*\text{A}|\text{D}^*\text{A}) \quad (2)$$

38
39
40
41
42
43
44
45 Because we assumed that the electron-transfer occurs in a gas phase, outer sphere
46
47 reorganization energy due to the solvent relaxation is not taken into account. In this
48
49 case, the total reorganization energy λ is equal to its inner sphere energy λ_i as:
50
51
52
53
54
55
56
57

$$\lambda = \lambda_i = E(\text{D}^{+\bullet}\text{A}^{-\bullet}|\text{D}^*\text{A}) - E(\text{D}^{+\bullet}\text{A}^{-\bullet}|\text{D}^{+\bullet}\text{A}^{-\bullet}) \quad (3)$$

1
2
3 A stabilization energy E_{st} was introduced to assess the stability of the charge-transfer
4
5
6 state ($D^{+\bullet}$ and $A^{-\bullet}$); larger values of E_{st} indicate higher stability of this state.
7
8
9

$$E_{st} = E(D^{+\bullet}|D^{+\bullet}) + E(A^{-\bullet}|A^{-\bullet}) - E(D^{+\bullet}A^{-\bullet}|D^{+\bullet}A^{-\bullet}) \quad (4)$$

10
11
12
13
14
15
16
17
18
19
20
21
22

23 **3. Results and Discussion**

24 25 **3.1 Structural Changes**

26
27
28
29 Figure 2 shows the optimized structures of **s1-s6**. Relative to their initial structures, no
30
31
32 significant changes of **s1-s4** were evident. However, the optimized structures of **s5** and **s6**
33
34
35 show slightly longer distances from NTz4T and NOz4T compared with their initial
36
37
38 structures.
39
40

41
42 Although NTz4T and NOz4T have slightly bent ground-state structures, they are almost
43
44
45 planar in the lowest-energy singlet excited state. The geometric difference between the
46
47
48 excited and radical cation states is not significant. Indeed, the root mean square deviation
49
50
51 (RMSD) of all atomic coordinates of **s1-s6** is 0.0155 Å for NTz4T and 0.0167 Å for
52
53
54 NOz4T. Additionally, there was little structural difference between the ground state of
55
56
57
58 PCBM and its radical anion.
59
60
61
62
63
64
65

1
2
3 We also calculated λ_{NTz4T} , λ_{NOz4T} , and λ_{PCBM} to evaluate the contribution of the
4
5
6 reorganization energy to the stability of the entire system. The respective average values
7
8
9 of all conformations (**s1-s6**) are $\overline{\lambda_{\text{NTz4T}}} = 8.38$ kJ/mol, $\overline{\lambda_{\text{NOz4T}}} = 9.06$ kJ/mol, and
10
11
12 $\overline{\lambda_{\text{PCBM}}} = 12.71$ kJ/mol. Clearly, PCBM contributes the most to the total reorganization
13
14
15 energy, and NOz4T has a slightly larger contribution than NTz4T.
16
17
18
19
20
21
22
23
24
25
26
27
28
29
30
31
32
33
34
35
36
37
38
39
40
41
42
43
44
45
46
47
48
49
50
51
52
53
54
55
56
57
58
59
60
61
62
63
64
65

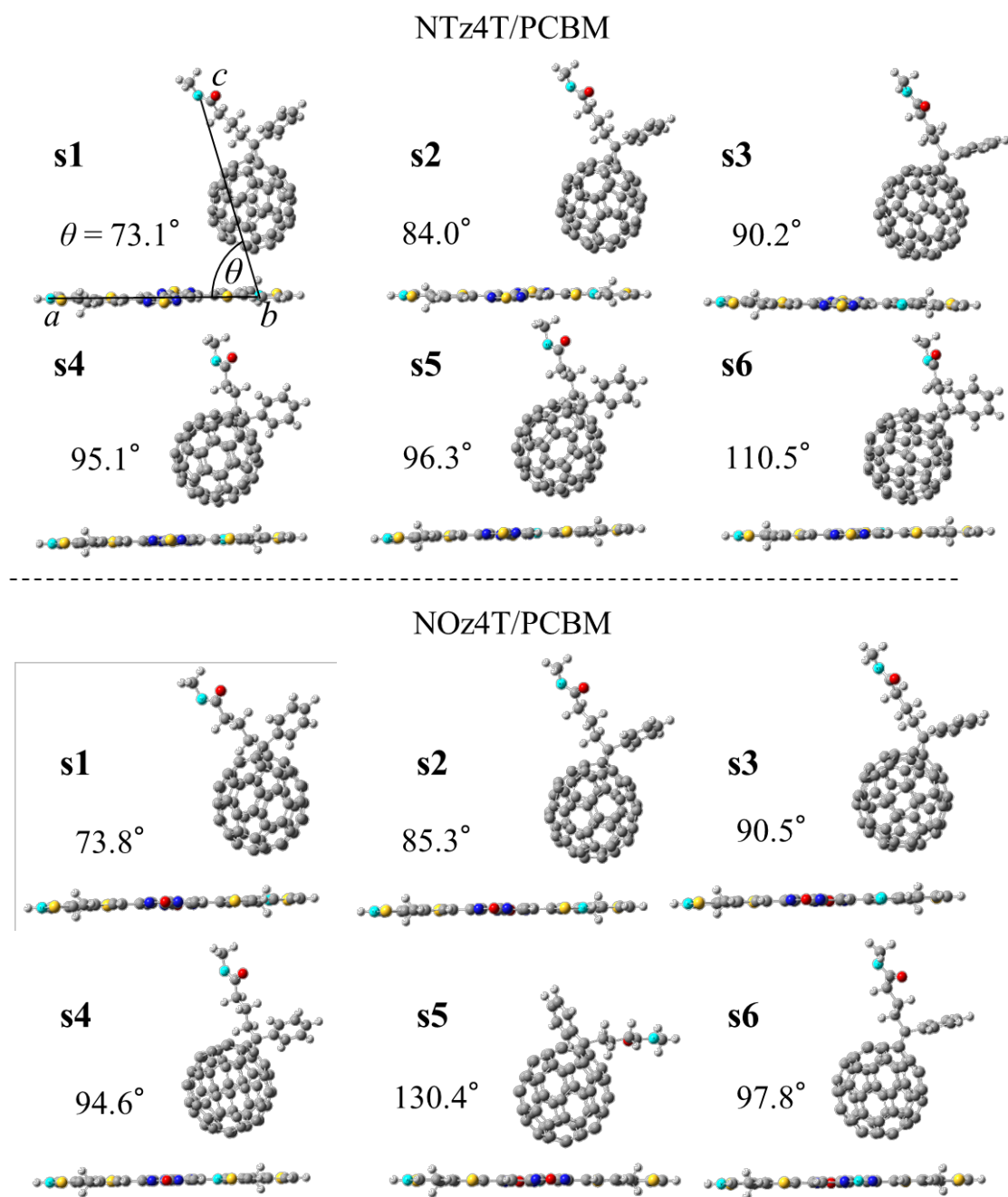


Figure 2. Fully optimized structures of **s1-s6**. The nearest intermolecular distance between the donor and acceptor atoms is almost identical to that of the initial structure. The angles (θ) between the cyan-coloured *a*, *b*, and *c* atoms are shown. *a*: terminal carbon atom of the NTz4T or NOz4T ring. *b*: nearest atom to PCBM. *c*: ether bonding

1
2
3 oxygen atom of PCBM. α of NOz4T/PCBM has an especially large angle because the
4
5
6 orientation of the functional groups of PCBM is reversed.
7
8
9

10 11 12 **3.2 Absorption Wavelengths and Molecular Orbitals**

13
14
15
16 We compared the absorption wavelengths (λ) of NTz4T and NOz4T at the TD-DFT level
17
18
19 of theory with the experimental values [9] to examine whether the singlet excited state
20
21
22 corresponds to the actual system. According to our calculations, the first
23
24
25 transition-allowed excited state could be attributed to a single electron excitation from the
26
27
28 HOMO to the lowest unoccupied molecular orbital (LUMO) of NTz4T and NOz4T
29
30
31 (Figure 3). Although the computed absorption wavelength was slightly shorter than the
32
33
34 experimental value (<50 nm), because of the short-conjugated monomer model [24], the
35
36
37 tendency is consistent with experimental results; that is, NTz4T has a shorter absorption
38
39
40 wavelength and weaker oscillator strength than NOz4T [9]. It is expected that excitation
41
42
43 of NOz4T occurs more efficiently than that of NTz4T because the oscillator strength of
44
45
46 the HOMO–LUMO excitation of NOz4T is larger than that of NTz4T (Figure 3).
47
48
49
50
51
52
53
54
55
56
57
58
59
60
61
62
63
64
65

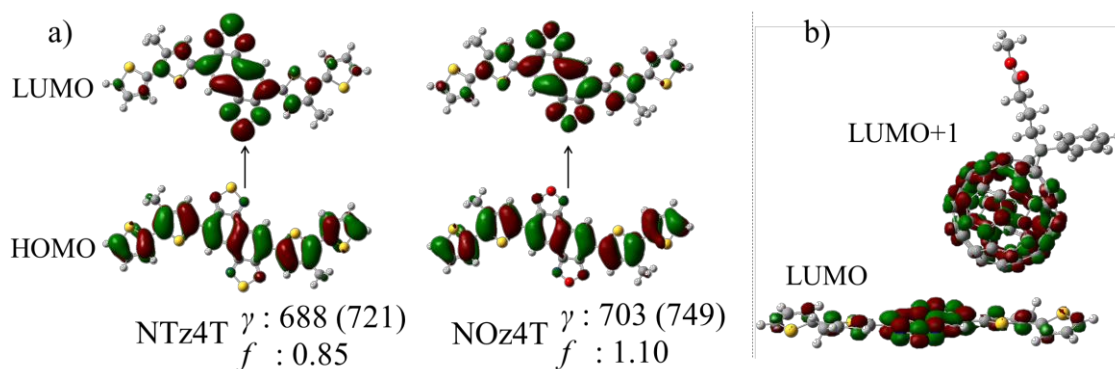


Figure 3. (a) HOMO/LUMO of NTz4T and NOz4T (isovalue of 0.020). The values of γ are given in nm, and the experimental values are shown in parentheses. The values of the absorption oscillator strength (f) are also given. (b) LUMO and LUMO+1 of NOz4T/PCBM (isovalue of 0.020), which are almost degenerate (<5 kJ/mol).

3.3 Calculated k_{ET} and E_{st}

Table 1 shows the k_{ET} and E_{st} of the systems and the three Marcus parameters. The overlap integrals between the donor and acceptor are shown in parentheses as a supplement to H_{ab} . For clarity, the qualitative differences of these were considered. Although efficient charge-transfer is expected in both models on the basis of k_{ET} , the NTz4T/PCBM model has a relatively larger k_{ET} than that of NOz4T/PCBM. These results reflect the high efficiency of PSCs using PNTz4T. Since the right-hand side of Eq. (1) contains $(\Delta G^0 + \lambda)^2$ in the exponential term, the k_{ET} difference between the models is mainly due to the difference between ΔG^0 and λ . The average ΔG^0 values in **s1-s6** in the

1
2
3 NTz4T/PCBM and NOz4T/PCBM models are -70.71 and -85.21 kJ/mol, respectively. As
4
5
6 for the average λ in **s1-s6**, we obtain 16.72 kJ/mol for NTz4T/PCBM and 19.76 kJ/mol for
7
8
9 NOz4T/PCBM. From these results, this reaction occurs in the inverted region of Marcus
10
11
12 theory for both models, and the large k_{ET} of NTz4T/PCBM is attributed to its small $(\Delta G^0$
13
14
15
16
17
18
19
20
21
22
23
24
25
26
27
28
29
30
31
32
33
34
35
36
37
38
39
40
41
42
43
44
45
46
47
48
49
50
51
52
53
54
55
56
57
58
59
60
61
62
63
64
65

Moreover, the k_{ET} values of **s4-s6** in NTz4T/PCBM tend to be much larger than those in
s1-s3, indicating that k_{ET} is conformation dependent. The primary difference between
s4-s6 and **s1-s3** is attributed to the difference in H_{ab} ; H_{ab} for **s4-s6** are ~100 times larger
than those of **s1-s3**. Therefore, we can speculate that conformation contributes to H_{ab} ,
which increases when the donor and acceptor couple strongly. The strength of the
coupling between the donor and acceptor is reflected in the value of the overlap integral,
which is increased when the MOs of the donor and acceptor are closer. Indeed, as shown
in Figure 3, the LUMOs in the ground state of NTz4T and NOz4T are localized in the
naphtho-bis-thiadiazole (NTz) and naphtho-bis-oxadiazole (NOz) moieties, and PCBM
in **s4-s6** is in the proximity of these orbitals. Therefore, the overlap integral becomes large
(Table 1), and strong coupling occurs between the donor and acceptor.

Although the same tendency is found in **s4-s6** of NOz4T/PCBM, the reorganization
energy has an important contribution to the large k_{ET} in **s5** and **s6**. In addition, the

1
2
3 calculated coupling constant for **s5** is very small. Structurally, PCBM is out of the ring
4
5
6 plane from the first step of the geometry optimization (Figure 4). The structural
7
8
9 specificity of **s5** can also be ascertained from its relatively large angle involving PCBM
10
11
12 and its counterpart (Figure 2). Although it differs from the assumed conformation, we can
13
14
15 gauge the magnitude of the contribution of λ by comparing **s5** with **s1-s3**.
16
17

18
19 The average value of E_{st} for the NTz4T/PCBM system (136.94 kJ/mol) is smaller than
20
21 that of NOz4T/PCBM (143.28 kJ/mol). This result suggests that the large E_{st} could be a
22
23 factor for lowering E_{loss} . E_{loss} is defined as $E_g - eV_{OC}$, where E_g is the bandgap, e is the
24
25 elementary charge, and V_{OC} is the open-circuit voltage. E_{st} is a value derived using the
26
27 total energy of the system, whereas E_{loss} is a value derived using the bandgap; comparing
28
29 these two values directly is therefore questionable. Nevertheless, the values of E_g as
30
31 derived from γ are 1.80 eV for PNTz4T and 1.76 eV for PNOz4T, which do not differ
32
33 considerably from the experimental values [9]. Although there is no research that reports
34
35 the correlation between E_{st} and E_g , or E_{st} and E_{loss} , these properties could have a negative
36
37 correlation with each other. We intend to confirm the correlation between E_{st} and E_g , and
38
39 subsequently E_{st} and E_{loss} , in future studies by increasing the number of calculation
40
41 targets.
42
43
44
45
46
47
48
49
50
51
52
53
54
55
56

57
58 Consistent with our expectations, **s4** and **s5** of NTz4T/PCBM have larger E_{st} values than
59
60

those of NOz4T/PCBM, because NTz4T has a large overlap integral with PCBM in these conformations. The same tendency is also observed in **s4** of NOz4T/PCBM.

Table 1. Calculated values of ΔG^0 , λ , $|H_{ab}|$, k_{ET} , and E_{st} , with the overlap integral between NTz4T/NOz4T and PCBM in parentheses.

	s1	s2	s3	s4	s5	s6
NTz4T/PCBM						
ΔG^0 ^a	-79.44	-78.35	-77.39	-55.95	-60.23	-72.87
λ ^a	15.52	15.43	16.11	18.77	15.52	18.95
$ H_{ab} $ ^a	0.49	0.14	0.43	17.76	16.24	10.70
	(0.006)	(0.002)	(0.006)	(0.167)	(0.149)	(0.095)
k_{ET} ^b	6.65×10^0	1.08×10^0	1.03×10^2	1.42×10^{12}	2.53×10^{11}	1.73×10^8
E_{st} ^a	133.23	135.26	136.05	155.85	154.09	143.23
NOz4T/PCBM						
ΔG^0 ^a	-86.23	-88.84	-86.27	-80.66	-86.39	-82.89
λ ^a	16.09	19.59	16.30	15.69	25.05	25.85
$ H_{ab} $ ^a	0.42	0.09	0.15	12.36	0.56	9.13
	(0.012)	(0.001)	(0.008)	(0.095)	(0.007)	(0.077)
k_{ET} ^b	6.67×10^{-2}	1.18×10^0	1.56×10^{-2}	2.34×10^3	5.74×10^5	1.95×10^9
E_{st} ^a	142.41	139.41	142.39	149.50	141.11	144.87

^a kJ/mol. ^b s⁻¹.

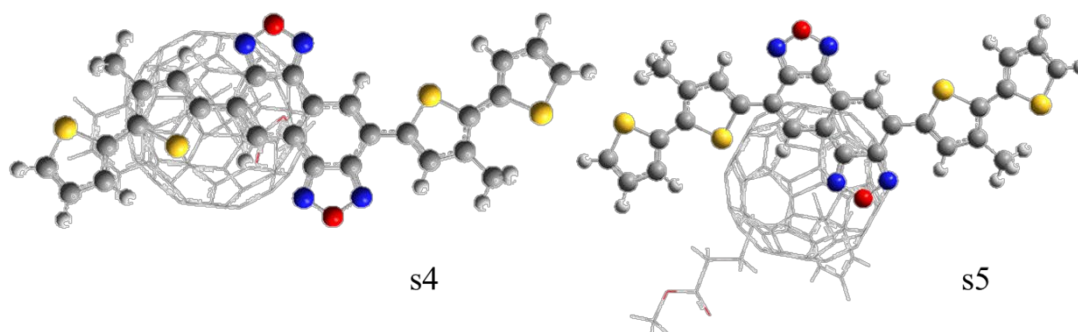


Figure 4. Structures of **s4** and **s5** (NOz4T/PCBM) viewed from the side of NOz4T.

NOz4T and PCBM are depicted by ball-and-stick and wireframe styles, respectively.

3.4 Discussion

Osaka *et al.* [9] have estimated that the driving force for the electron-transfer reaction at the PNOz4T/PCBM interface is ~ 12 kJ/mol on the basis of the energy gap between the LUMO of the donor and acceptor (ΔE_L). Its corresponding PCE is $\sim 9\%$, which implies that this reaction is efficient. However, the driving force of 12 kJ/mol is smaller than the empirically known threshold value [25] of 0.30 eV (~ 30 kJ/mol) for efficient electron-transfer, indicating that the PNOz4T/PCBM interface is an exception to the rule suggested in Ref. 25. In this study, the driving force at the PNOz4T/PCBM interface was estimated by using the total energy of the system, and a sufficient driving force was attained even in the PSC using PNOz4T.

The results show that a semiconducting polymer with a high PCE has a large k_{ET} and that

1
2
3 a small energy loss has a large E_{st} . Therefore, a semiconducting polymer with an
4
5
6 improved PCE and small E_{loss} has both a large k_{ET} and E_{st} .
7

8
9 λ and ΔG^0 contribute greatly in determining the magnitude of k_{ET} . Since the sum of λ and
10
11 ΔG^0 is negative, the reactions assumed in this study occur in the Marcus inverted region.
12
13 Here, k_{ET} increases with an increase of λ or a decrease of $|\Delta G^0|$ (Figure 5). Because the
14
15 correlation between ΔG^0 and λ is relatively weak, we conclude that these parameters are
16
17 mutually independent. In contrast, ΔG^0 and E_{st} are correlated through the energy of the
18
19 charge-transfer state $E(D^{+\bullet}A^{\bullet-} | D^{+\bullet}A^{\bullet-})$. Therefore, semiconducting polymers should be
20
21 designed by focusing on lowering the energy of the lowest-energy singlet excited state
22
23 $E(D^*A | D^*A)$ to decrease the absolute value of ΔG^0 without affecting E_{st} ; that is,
24
25 semiconducting polymers with a narrow bandgap are preferable. However, polymers that
26
27 experience large structural changes before and after charge-transfer should be considered
28
29 to increase λ .
30
31
32
33
34
35
36
37
38
39
40
41
42
43
44
45
46
47
48
49
50
51
52
53
54
55
56
57
58
59
60
61
62
63
64
65

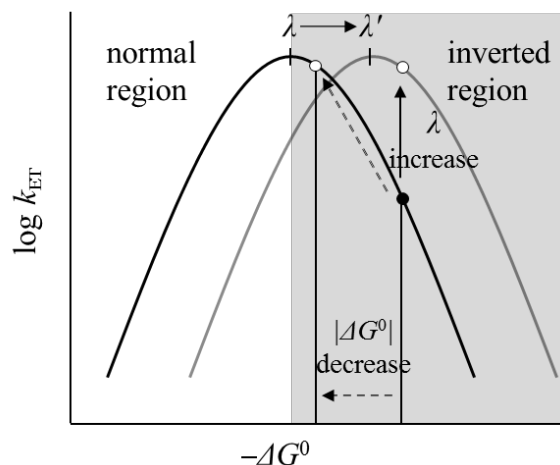


Figure 5. Conceptual diagram of the Marcus curve. Solid and dotted arrows represent the direction of the λ increase and $|\Delta G^0|$ decrease, respectively. The filled and open dots indicate plots of the actual and ideal systems, respectively.

To improve E_{st} , increasing the contribution of charge delocalization (i.e. expanding the π -conjugated system) seems to be effective. Because E_{st} also tends to increase as H_{ab} increases, it is also conceivable to design a semiconducting polymer with a spatially delocalized LUMO in the ground state.

4. Conclusion

This study investigated the electron-transfer rate constant (k_{ET}) by Marcus theory and the stabilization energy of the charge-transfer state (E_{st}) for each conformation of the NTz4T/PCBM and NOz4T/PCBM models at the CDFT level. A high PCE is predicted

1
2
3 for NTz4T/PCBM with a large k_{ET} , and NOz4T/PCBM with a large E_{st} has a small E_{loss} .
4
5

6 In the **s4-s6** conformations where PCBM exists above the NTz and NOz moieties, the
7
8 LUMO in the ground state of the donor has a large overlap integral with the acceptor,
9
10 resulting in a large k_{ET} . Therefore, we found that NOz and NTz, as introduced into a
11
12 semiconducting polymer by Osaka *et al.*, greatly contribute to enhancing the efficiency of
13
14 electron-transfer.
15
16
17
18
19
20
21

22 It was also found that the PSC based on PNOz4T possesses a satisfactory driving force
23
24 for electron-transfer, as estimated from the total energy of the system. Overall, our
25
26 computational results support the high efficiency of PSCs based on PNOz4T, and the
27
28 scheme introduced by Wu *et al.* is applicable for estimating electron-transfer reactions in
29
30 PSCs. We expect that their scheme is effective to the electron-transfer reactions of other
31
32 PSC systems as well.
33
34
35
36
37
38
39
40
41

42 In order to develop semiconducting polymers with effectual PCE and small E_{loss} , it is
43
44 necessary to increase the magnitudes of both k_{ET} and E_{st} . The requirements to improve the
45
46 performance of semiconducting polymers include: (i) large structural changes through
47
48 charge-transfer to enhance λ , (ii) narrow band gap to lower the driving force, and (iii)
49
50 spatially delocalized LUMO of the ground state to increase electronic coupling.
51
52
53
54
55
56
57
58
59
60
61
62
63
64
65

1
2
3 **Acknowledgements**
4
5

6 This study was supported by Grants-in-Aid for Scientific Research (B) (No. 17H03034)
7
8
9 from the Japanese Society for the Promotion of Science (JSPS). Some calculations were
10
11
12 performed at the Research Center for Computational Science (RCCS), Okazaki Research
13
14
15 Facilities, and National Institutes of Materials Sciences (NIMS).
16
17
18
19
20
21
22
23
24
25
26
27
28
29
30
31
32
33
34
35
36
37
38
39
40
41
42
43
44
45
46
47
48
49
50
51
52
53
54
55
56
57
58
59
60
61
62
63
64
65

1
2
3 **References**
4
5

- 6 [1] I. Osaka, M. Shimawaki, H. Mori, I. Doi, E. Miyazaki, T. Koganezawa, K. Takimiya,
7
8 J. Am. Chem. Soc. 134 (2012) 3498.
9
10
11 [2] B. Liu, E. S. Aydil, J. Am. Chem. Soc. 131 (2009) 3466.
12
13
14 [3] M. Wang, H. Wang, T. Yokoyama, X. Liu, J. Am. Chem. Soc. 136 (2014) 12576.
15
16
17 [4] A. Pivrikas, N. S. Sariciftci, G. Juska, R. Osterbacka, Prog. Photovolt: Res. Appl. 15
18
19 (2007) 677.
20
21
22 [5] G. Yu, J. Gao, J. C. Hummelen, Science 270 (1995) 1789.
23
24
25 [6] A. Facchetti, Mater. Today 16 (2013) 123.
26
27
28 [7] Y. Liang, Z. Xu, J. Xia, Adv. Mater. 22 (2010) 135.
29
30
31 [8] V. Vohra, K. Kawashima, T. Kakara, T. Koganezawa, I. Osaka, K. Takimiya, H.
32
33 Murata, Nat. Photonics 9 (2015) 403.
34
35
36 [9] K. Kawashima, Y. Tamai, H. Ohkita, I. Osaka, and K. Takimiya, Nat. Commun. 6
37
38 (2015) 10085.
39
40
41 [10] I. Ciofini, C. Adamo, H. Chermette, Chem. Phys. 309 (2005) 67.
42
43
44 [11] P. H. Dederichs, S. Blugel, R. Zeller, H. Akai, Phys. Rev. Lett. 53 (1984) 2512.
45
46
47 [12] B. Kaduk, T. Kowalczyk, and T. V. Voorhis, Chem. Rev. 112 (2012) 321.
48
49
50 [13] R. A. Marcus, J. Chem. Phys. 24 (1956) 966.
51
52
53
54
55
56
57
58
59
60
61
62
63
64
65

- 1
2
3 [14]Q. Wu, T. V. Voorhis, J. Phys. Chem. A 110 (2006) 9212.
4
5
6 [15]T. Ogawa, M. Sumita, Y. Shimodo, K. Morihashi, Chem. Phys. Lett. 511 (2011)
7
8
9 219.
10
11
12 [16]K. Aikawa, M. Sumita, Y. Shimodo, K. Morihashi, Phys. Chem. Chem. Phys. 17
13
14 (2015) 20923.
15
16
17 [17]K. Aikawa, T. Matsui, K. Morihashi, Chem. Lett. 45 (2016) 628.
18
19
20 [18]Q. Wu, T. V. Voorhis, J. Chem. Phys. 125 (2006) 164105.
21
22
23 [19]J. C. Hummelen, B. W. Knight, F. LePeq, F. Wudl, J. Org. Chem. 60 (1995) 532.
24
25
26 [20]A. D. Becke, J. Chem. Phys. 98 (1993) 5648.
27
28
29 [21]GAUSSIAN 09, Revision D. 01, M. J. Frisch, *et al.*, Gaussian Inc. Wallingford CT,
30
31 200
32
33
34 [22]E. Runge, E. K. U. Gross, Phys. Rev. Lett. 52 (1984) 997.
35
36
37 [23]R. A. Marcus, N. Sutin, Biochem. Biophys. 811 (1985) 265.
38
39
40 [24]T. Matsui, Y. Imamura, I. Osaka, K. Takimiya, T. Nakajima, J. Phys. Chem. C 120
41
42 (2016) 8305.
43
44
45 [25]M. C. Scharber, D. Muhlbacher, M. Koppe, Adv. Mater. 18 (2006) 789.
46
47
48
49
50
51
52
53
54
55
56
57
58
59
60
61
62
63
64
65